European Polymer Journal 44 (2008) 1613–1619

Contents lists available at ScienceDirect

European Polymer Journal

journal homepage: www.elsevier.com/locate/europolj

Macromolecular Nanotechnology

A novel method for preparation of exfoliated UV-curable polymer/clay nanocomposites

Shichang Lv [a], Wei Zhou [a], Song Li [b], Wenfang Shi [a,*]

[a] Department of Polymer Science and Engineering, Joint Laboratory of Polymer Thin Films and Solution, University of Science and Technology of China, Hefei, Anhui 230026, PR China
[b] Department of Chemistry, University of Science and Technology of China, Hefei, Anhui 230026, PR China

ARTICLE INFO

Article history:
Received 7 November 2007
Received in revised form 26 March 2008
Accepted 2 April 2008
Available online 8 April 2008

Keywords:
Nanocomposites
Montmorillonite
UV-curable
Exfoliation

ABSTRACT

The half adduct of isophorone diisocyanate and 2-hydroxyethyl acrylate (IPDI-HEA), as a reactive organic modifier, was used to functionalize Na-montmorillonite (Na-MMT) clay. Unlike the electronic interaction in the conventional cation-exchange method, the driving force for the organic modification came from the chemical reaction between IPDI-HEA and framework hydroxyl groups on the surface of clay. With high degree of organic modification (48%), the *d*-spacing of clay layer was greatly enlarged to 3.32 nm, and the clay became more organophilic. After in situ photopolymerization among the IPDI-HEA grafted MMT clay, monomers and oligomers, the exfoliated polymer/clay nanocomposites were obtained. X-ray diffraction and transmission electron microscopy were used to detect the structure and morphology of the clay dispersed in the polymer matrix. Compared with the pure polymer materials, the exfoliated polymer/clay nanocomposites exhibited enhancements in mechanical and thermal properties.

1. Introduction

Polymer/clay nanocomposites have been studied extensively over the last decade for their unique properties compared to those of conventional composites, such as better mechanical and thermal properties [1–4], improved barrier properties, and enhanced chemical stability [5–7]. Since the first work done by researchers at Toyata Research Center on exfoliated nylon/clay nanocomposites [8], many kinds of polymers have been introduced to this field for the preparation of p\olymer/clay nanocomposites, such as epoxy [2,9–15], polycaprolactone [16], polystyrene [17,18], poly (ethylene oxide) [7,19], polyimide [20], and polymethylmethacrylate [21,22]. As mentioned above, most of them are thermally cured polymers.

UV-curable materials are increasingly applied in various scientific and industrial fields, because the UV-curing technology offers many advantages, such as solvent-free, low energy consuming, short time processing, and so on. While a lot of studies have been done on thermal curable polymer systems, only few are for the preparation of UV-curable polymer/clay nanocomposites. Zahouily et al. prepared the UV-curable urethane polymer/clay nanocomposites based on organo-modified clay for the first time [23,24], and used X-ray diffraction method to confirm the presence of exfoliated nanometer-thick clay platelets. Uhl et al. reported a variety of UV-curable urethane polymer/clay nanocomposites by using commercial clays and monomers as well as oligomers [25–27]. Dean et al. investigated the differences between the active silane-grafted and ion-exchanged organo-clays for their applications in photoinitiated polymerized polymer/clay nanocomposites [28].

* Corresponding author. Tel.: +86 551 3606084; fax: +86 551 3606630.
E-mail address: wfshi@ustc.edu.cn (W. Shi).

0014-3057/$ - see front matter © 2008 Elsevier Ltd. All rights reserved.
doi:10.1016/j.eurpolymj.2008.04.005

A difficult problem to be solved during the preparation of polymer/clay nanocomposites is that the presence of polar hydroxyl groups on the clay surface impedes the non-polar polymer chains to enter the galleries, so few exfoliated materials can be achieved. In order to well disperse inorganic clay fillers in the organophilic polymer matrix, one frequently used method is to replace the alkaline cations with alkylammonium cations by cation-exchange. One promising strategy is to explore some new reactive group-contained alkylammonium surfactants to modify clays. However, the surfactants containing both alkylammonium and some other reactive groups (epoxy, acrylate et al.) are hard to obtain.

It is worth to develop new universal methods using organic modifiers to treat the natural clay and produce exfoliated polymer/clay nanocomposites. In this paper, we demonstrate a novel method for the preparation of exfoliated nanocomposite based on the organo-modified clay with reactive acrylate group grafted to the clay layer by covalent bonds. Firstly, through the cation-exchange, the long alkyl chain of cetyltrimethyl ammonium bromide (CTAB) is intercalated into Na-MMT clay galleries and enlarges the layer spacing to get CTAB-MMT clay. For the intercalation of isophorone diisocyanate terminated 2-hydroxyethyl acrylate (IPDI-HEA) to the CTAB-MMT clay layer, toluene is used as a medium to avoid the moisture during the reaction between isocyanate groups and framework hydroxyl groups of the silicate layer, thus the CTAB-MMT clay precursor is functionalized with acrylate groups, and the obtained clay is named as IH-MMT clay. The clay gets more organophilic and also the layer spacing distance becomes larger which facilitates the exfoliating of the clay. Finally, the exfoliated UV-curable polymer/clay nanocomposites are obtained by photopolymerization among IH-MMT clay, monomers and oligomers. To avoid the aggregation of clay in the conventional dry and milling process, the azeotropy method is first used to make a solvent-transfer process in the reaction.

2. Experimental

2.1. Materials

Sodium montmorillonite (Na-MMT) with cationic exchange capacity (CEC) of 90 mEq/100 g was provided by FengHong Co., Zhejiang, China. Cetyltrimethyl ammonium bromide (CTAB) and toluene were purchased from China National Medicine Group (Shanghai Chemical Reagents Co.). The detailed synthesis and characterization of half adduct of isophorone diisocyanate and 2-hydroxyethyl acrylate (IPDI-HEA) were described elsewhere [29]. EB270, an aliphatic polyurethane acrylate with an unsaturation concentration of 1.33 mmol g^{-1} and a molar mass of 1500 g mol^{-1}, and 1, 6-hexamethyldiol diacrylate (HDDA) were supplied by Cytec Industries Inc. (USA). 1-Hydroxycyclohexyl-phenyl ketone (Runtecure 1104), used as a photoinitiator, was supplied by Runtec chemicals Co., Changzhou (China). All chemicals were used as received without further purification.

2.2. Clay modification

2.2.1. Preparation of CTAB-MMT clay

The organophilic montmorillonite, referred as CTAB-MMT, was obtained through a cation-exchange process as follows. 4.0 g Na-MMT was dispersed in 1000 mL distilled water with vigorous mechanical stirring to form a uniformly suspended solution. An excessive amount of cetyltrimethyl ammonium bromide (CTAB) aqueous solution was added to the Na-MMT suspended solution and stirred vigorously at 80 °C overnight to carry out the cationic exchange. The obtained modified clay was washed repeatedly with distilled water until no AgBr precipitate was found by titrating the filtrate with 0.1 N $AgNO_3$ solution. A desired mount of the solution was centrifuged and dried for characterization.

2.2.2. Preparation of IH-MMT clay

A proper amount of water suspension containing 2.0 g CTAB-MMT was dispersed in 150 mL of toluene, then water was removed by azeotropy. After the temperature cooled down to room temperature, an excess amounts of IPDI-HEA (50 mmol), a proper portion of catalyst (0.1 wt% DBTDL) and *p*-hydroxyanisole (1000 ppm) were added to the above vessel and stirred vigorously at 70 °C for different times (12, 24, 36, 48, 60, 72 h) under N_2 atmosphere. The product was collected by filtrating and then repeatedly washed with toluene to remove unreacted IPDI-HEA. The obtained functionalized clays reacted for 12, 24, 36, 48 h were named as IH-MMT-12, IH-MMT-24, IH-MMT-36, IH-MMT-48, respectively. The IH-MMT-48 was dispersed in toluene to obtain a suspension.

2.3. Preparation of polymer/IH-MMT nanocomposites

Polymer film formulation utilized in this study was a 7:3 mixture of EB270:HDDA. The clay loadings in these systems were 1, 3, 5 wt%, respectively. A desired amount of HI-MMT-48 toluene suspension was first dispersed in the EB270/HDDA formulation. After stirring vigorously for 24 h to achieve the complete dispersion, toluene was removed under vacuum. Then, 1.5 wt% radical fragmental photoinitiator (Runtecure 1104), based on the weight of formulation, was added, sealed in dark and stirred in N_2 atmosphere at room temperature for 2 h to prevent unexpected reactions. The films were applied to glass substrates, and finally exposed to a medium pressure mercury lamp (1 kW, Fusion UV systems, USA) with the band conveyer speed of 2.0 m min^{-1}. The UV-cured films of polymer/IH-MMT nanocomposites were obtained, referred as NC1, NC3 and NC5 with the IH-MMT-48 loadings of 1, 3, 5 wt%, respectively. The incident light intensity on the sample was measured to be 30 mW cm^{-2} with a UV power meter.

For comparison of the morphology and dispersion of the organo-modified clays in the polymer matrix, the nanocomposites filled with CTAB-MMT clay were also prepared under the same procedure as that of polymer/IH-MMT nanocomposites.

2.4. Characterization

The X-ray diffraction (XRD) patterns were recorded using a Rigaku D/Max-rA rotating anode X-ray diffractometer equipped with a Cu Kα tube and Ni filter (λ = 0.1542 nm). The Fourier transfer infrared (FTIR) spectra were recorded using a Nicolet MAGNA-IR 750 spectrometer with a KBr disk or thin film. The transmission electron microscope (TEM) and high resolution TEM micrographs were obtained with a Hitachi (Tokyo, Japan) H-800 and JEOL-2011, respectively, operated both at an acceleration voltage of 200 kV. The samples were ultramicrotomed with a diamond knife on a LKB Pyramitome to give 60-nm thick slices. The thermogravimetric analysis (TGA) was performed on a Shimadzu TGA-50 H thermoanalyzer. In each case a 10-mg sample was examined under a N_2 flow rate of 6×10^{-5} m^3/min at a heating rate of 5 °C/min from room temperature to 700 °C. The photopolymerization rate was monitored in air by a CDR-1 differential scanning calorimeter (DSC) (Shanghai Balance Instrument Co., Shanghai, China) equipped with a UV spot cure system BHG-250 (Mejiro Precision Co., Japan). The incident light intensity at the sample pan was measured to be 2.4 mW cm^{-2} with a UV power meter. The unsaturation conversion (P_t) was calculated by the formula, $P_t = H_t/H_\infty$, where H_t is the heat effect within t (s), H_∞ is the heat effect of 100% unsaturation conversion. The DSC curves were normalized by the weight (g) of samples. The polymerization rate is defined by $mmol_{c=c}\ g^{-1}\ s^{-1}$, namely, the variation of unsaturation concentration ($mmol_{c=c}\ g^{-1}$) per second. For calculating the polymerization rate and H_∞, the value, ΔH_0 = 86 J $mmol^{-1}$, for the heat of polymerization per acrylate unsaturation was taken. The tensile storage modulus (E') and tensile loss factors ($\tan\delta$) of UV-cured films were measured by a dynamic mechanical thermal analyzer (Diamond DMA, PE Co., USA) at a frequency of 10 Hz and a heating rate of 5 °C/min in the range of −100 to 200 °C with the sheets of $25 \times 5 \times 1$ mm^3. The crosslink density (v_e) as the molar number of elastically effective network chain per cube centimeter of the film, was calculated from the storage modulus in the rubbery plateau region according to: $v_e = (E'/3RT)$, where E' is the elastic storage modulus, R is the ideal gas constant, and T is the temperature in K. The mechanical properties were measured with an Instron Universal tester (model 1185, Japan) at 25 °C with a crosshead speed of 25 mm min^{-1}. The dumb-bell shaped specimens were prepared according to ASTM D412-87. Five samples were analyzed to determine an average value in order to obtain the reproducible result. The abrasion resistance was measured with a QMX abrasion apparatus (Tianjin Exp. Apparatus Co., China) in accordance with the corresponding State Standard Testing Method (GB 1731-93). The pendulum hardness of the cured films was determined in the Persoz mode in seconds by using a QBY pendulum apparatus (Tianjin Instrument Co., China). The pencil hardness of the cured films was determined using a QHQ-A pencil hardness apparatus (Tianjin Instrument Co., China).

3. Results and discussion

3.1. Clay modification

The evidence for the intercalation of CTAB and IPDI-HEA to the Na-MMT clay comes from FTIR, XRD and TGA studies. The FTIR spectra of Na-MMT, cation-exchanged and IPDI-HEA functionalized clays are shown in Fig. 1, with their characteristic peaks summarized in Table 1. It can be seen that all samples display the typical framework –OH stretching absorption at 3627 cm^{-1}. For CTAB-MMT, the peaks at 2850 and 2920 cm^{-1} can be assigned to the stretching vibration for $-CH_2$ and $-CH_3$, indicating the presence of long alkyl chain in the clay. Compared to CTAB-MMT, IH-MMT-48 shows new absorption peaks at 3382 and 1534 cm^{-1} for N–H stretching and bending vibrations, respectively. Two stretching bands of C=O and C=C of acrylate group appear at 1724 cm^{-1}, and at 1640, 1412, 810 cm^{-1}, respectively. These FTIR assignments demonstrate that IPDI-HEA had been grafted to the CTAB-MMT clay layer.

The powder X-ray diffraction patterns for Na-MMT and organo-modified clays are shown in Fig. 2. The unmodified Na-MMT shows a primary silicate (1 0 0) reflection at 5.78°, corresponding to a d-spacing of 1.52 nm. Upon the first organic modification, an increase in the interlayer spacing is observed. The enlarged d-spacing (2.11 nm) of CTAB-MMT indicates the successful intercalation of cetyltrimethyl ammonium cation into the Na-MMT layer via cation-exchange, thus making silicates organophilic and facilitating the intercalation of IPDI-HEA. For IH-MMTs, as listed in Table 2, with prolonging the time of reaction between IPDI-HEA and CTAB-MMT, the d-spacing increases from 2.27 nm for IH-MMT-12 to 3.32 nm for IH-MMT-48. Whereas further increasing the reaction time would not enlarge the d-spacing of clay layer any more, which confirms that the reaction has proceeded to completion.

The thermogravimetric analysis (TGA) in N_2 was used to determine the contents of organo-modifiers and other volatile materials (e.g. water) in the samples. As shown in Fig. 3, for Na-MMT, a weight loss of 13% is observed when heating between 30 °C and 200 °C, which should be related

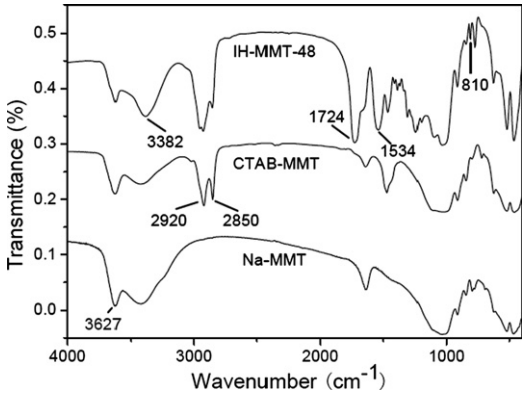

Fig. 1. FTIR spectra of Na-MMT and modified clays.

Table 1
Characteristic FTIR peaks for MMT modifications

Groups		Wavenumbers (cm^{-1})
Organic	$-CH_2$, $-CH_3$	2920, 2850
	C=C	1640, 1412, 810
	C=O	1724
	N–H	3382, 1534
	C–N	1385
Silicate	Framework OH stretch	3627
	Interlayer H_2O stretch	3425
	H–O–H def	1640
	Si–O stretch	1116, 1034, 914

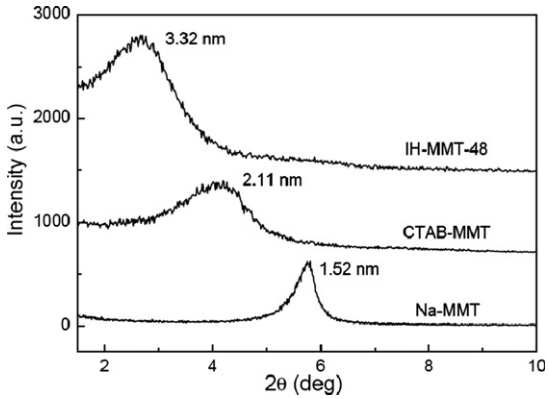

Fig. 2. XRD patterns of Na-MMT and modified clays.

Table 2
XRD d_{100}-spacings for Na-MMT, CTAB-MMT and IH-MMTs

Sample	Basal spacing d_{100} (nm)	% Increase in d-spacing relative to Na-MMT
Na-MMT	1.52	Not applicable
CTAB-MMT	2.11	39
IH-MMT-12	2.27	49
IH-MMT-24	2.67	76
IH-MMT-36	3.10	104
IH-MMT-48	3.32	118

to the loss of water physically adsorbed to the Na-MMT layer. The weight loss between 180 °C and 410 °C (26.9% for CTAB-MMT, and 61.9% for IH-MMT-48) is attributed to the decomposition and combustion of the intercalated organomodifiers. When heating to 700 °C, the weight residuals of the clays are 82.3% for Na-MMT, 65.1% for CTAB-MMT and 28.5% for IH-MMT-48. As the isocyanate group of IPDI-HEA can only react with the framework hydroxyl groups, it is expected that a high percentage of IPDI-HEA should be present in IH-MMT-48 sample. The result demonstrates that, with increasing the degree of modification, the d-spacing of clay might effectively increased, which is in agreement with the XRD result.

3.2. Morphology and dispersion of modified clays in nanocomposites

The XRD patterns of polymer/CTAB-MMT and polymer/IH-MMT nanocomposites at 5 wt% clay loading are presented in Fig. 4. It should be noted that the absence of XRD diffraction peaks does not equally mean the occurrence of exfoliation, as the observed absence of diffraction peak could be due to the lack sensitivity at the lower amount of clay loading or random orientation of clay tactoids. For the polymer/CTAB-MMT nanocomposite at 5 wt% loading, there is a weak peak observed at 3.87° corresponding to the d-spacing of 2.28 nm, which is slight larger than that of CTAB-MMT clay (2.11 nm), indicating that few polymer chains had been intercalated into the clay layer during the photopolymerization process, and an intercalated structure was formed. However, the cation-exchange organo-modification alone is not sufficient to exfoliate the clay layer. For polymer/IH-MMT nanocomposite, no peak within the range can be observed, indicating that exfoliated nanocomposite might be present as opposed to polymer/CTAB-MMT nanocomposite.

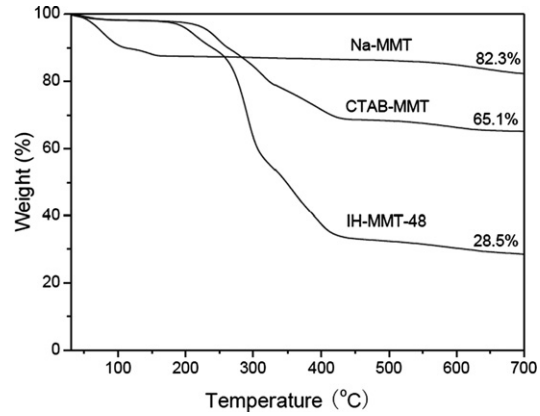

Fig. 3. TGA curves of Na-MMT and modified clays.

For confirming the formation of exfoliated structure in the polymer/IH-MMT nanocomposite, the TEM micrographs are shown in Fig. 5 with the samples at 5 wt% clay loading. The dark lines are intersections of clay platelets. It is well known that, while XRD analysis gives the macroscopic conformation of a sample, TEM photograph shows the local microscopic conformation. For polymer/CTAB-MMT nanocomposite, the large particle aggregates are

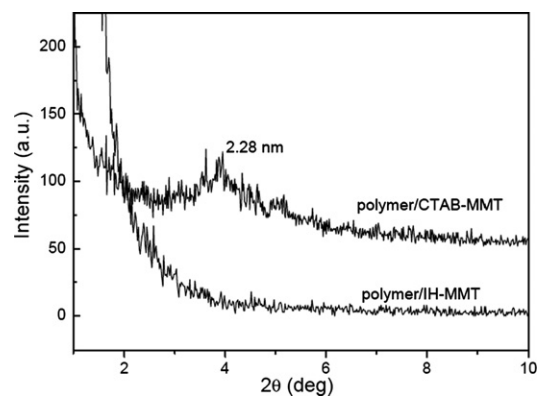

Fig. 4. XRD patterns of polymer/CTAB-MMT and polymer/IH-MMT nanocomposites at 5 wt% clay loading.

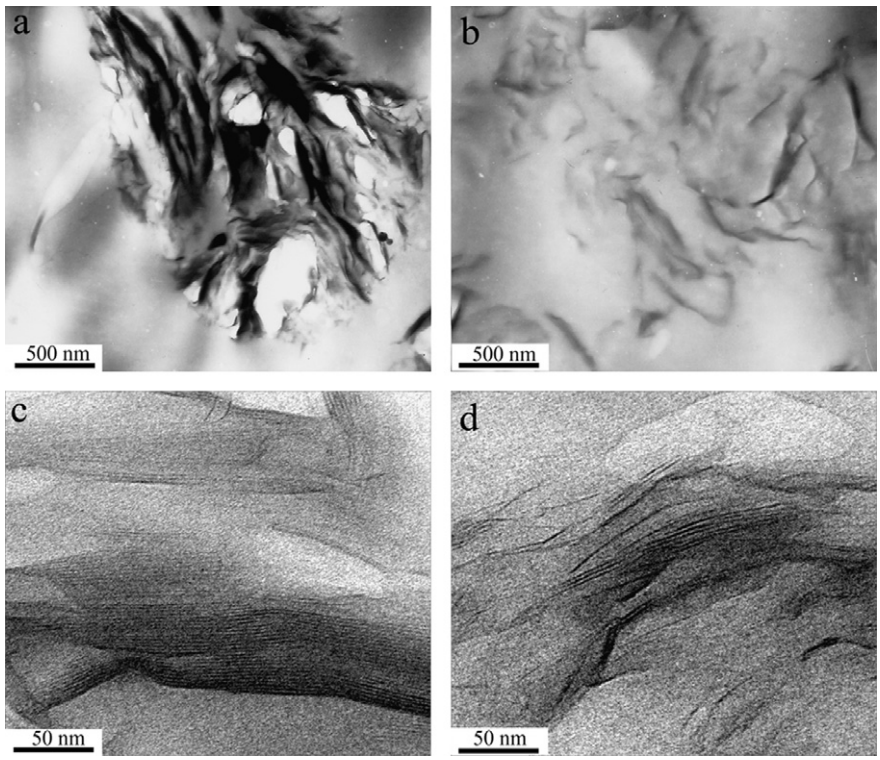

Fig. 5. TEM and HRTEM micrographs of polymer/CTAB-MMT (a, c) and polymer/IH-MMT nanocomposites (b, d) at 5 wt% clay loading.

observed under lower magnification (Fig. 5a), indicating that the clay particles are neither well-exfoliated nor dispersed uniformly in the polymer matrix. The HRTEM observation further demonstrates that these aggregates are comprised of dozens of clay platelets (Fig. 5c). However, the polymer/IH-MMT nanocomposite shows good dispersion of clay in the polymer matrix (Fig. 5b) and a completely different morphology. The clay was exfoliated into thin tactoids which only contain few clay layer(Fig. 5d). These thin tactoids dispersed uniformly and randomly during the curing process because the clay was previously modified by CTAB and then IPDI-HEA. The second organo-modification makes the layer distance large enough for exfoliation. Whereas for polymer/CTAB-MMT nancocomposite, the polymer chains can only be intercalated to the layer, without the formation of exfoliated structure.

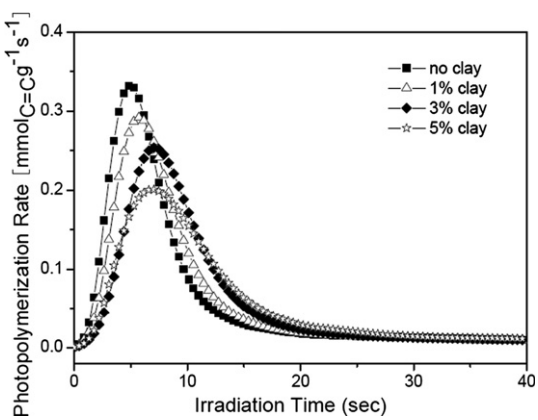

Fig. 6. Photopolymerization rates of pure polymer and polymer/IH-MMT nanocomposites.

3.3. Properties of UV-cured polymer/IH-MMT nanocomposite film

The properties of a UV-cured film depend on not only the resin composition but also the photopolymerization kinetics. In order to investigate the effects of the organo-modified clays on the photopolymerization kinetics, the photopolymerization rate at the peak maximum (R_p^{max}) and the final degree of double bond conversion (P^f) were measured, as shown in Figs. 6 and 7, respectively. For polymer/ IH-MMT nanocomposites, with increasing the clay content, the R_p^{max} decreases slightly and the longer irradiation time is needed to reach to R_p^{max}. This can be attributed to the lower concentration of double bond, and high viscosity compared with the pure resin. Moreover, the final unsaturation conversion also decreases with increasing the clay content, but leveling to acceptable values. This indicates the better compatibility between IH-MMT clays and the organic phases.

The TGA curves of pure polymer and polymer/IH-MMT nanocomposite samples are shown in Fig. 8. As indicated in the figure, the thermal behavior of the nanocomposite is quite similar to the pure polymer up to a loading of 5 wt%. However, the addition of the clay raises the onset temperature of thermal decomposition, resulting in the delayed thermal decomposition. When 5% weight loss is

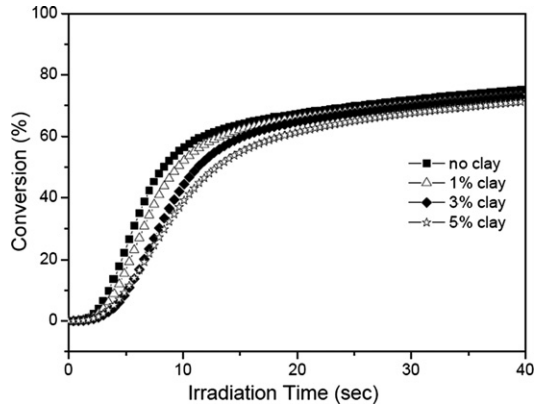

Fig. 7. Unsaturation conversion of pure polymer and polymer/IH-MMT nanocomposites.

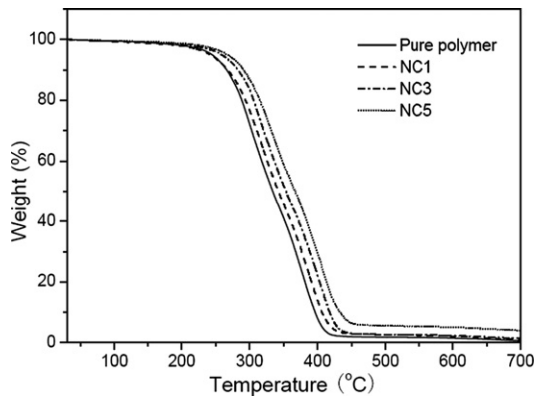

Fig. 8. TGA curves of pure polymer and polymer/IH-MMT nanocomposites under N_2 flow.

selected as a point of comparison, the decomposition temperatures for pure polymer, NC1, NC3, and NC5 samples are determined to be 244, 242, 259 and 267 °C, respectively. As the clay contents increases from 1 to 5 wt%, the increase of 0.9–4.0% of the char residue is also obtained, which means that the IH-MMT clay can promote the charring process during the degradation process. It can be clearly found from the figure that the thermal stability of polymer/IH-MMT nanocomposite films was improved with the addition of IH-MMT, which can be explained by the incorporation of IH-MMT clay to the polymer matrix.

Dynamic mechanical thermal analysis (DMTA) was utilized to investigate the mechanical properties in an effort to further examine the microstructures of cured films. The storage modulus (E') and tan δ curves of the pure polymer and its corresponding nanocomposites are shown in Fig. 9. The glass transition temperature (T_g) is defined as the peak temperature of tan δ curve. The storage modulus (E') of the nanocomposite increases with increasing the clay concentration, while T_g values for the nanocomposites are approximately the same as the pure polymer film. As listed in Table 3, as the amount of clay loading increases, the crosslink density (XLD) increases even though the R_p^{max} and conversion are lower for the nanocomposites than the pure resin. It can be explained that the effective degree

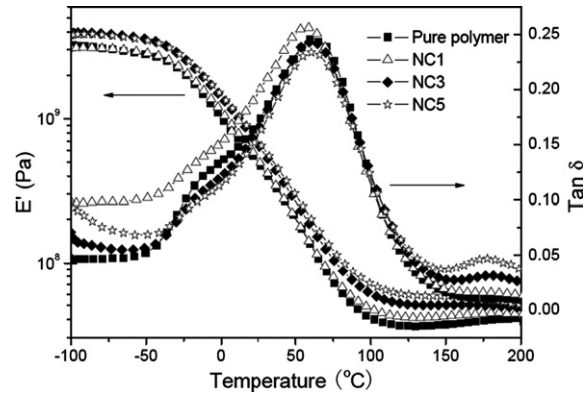

Fig. 9. DMTA curves of pure polymer and polymer/IH-MMT nanocomposites.

Table 3
Rubbery storage modulus, T_g and crosslink density (XLD) from DMTA

Sample	Rubbery storage modulus E' (Pa)	T_g (°C)	XLD (mol/cm^3)
Pure polymer	3.69×10^7	59.8	3.67×10^{-3}
NC1	4.20×10^7	58.8	4.18×10^{-3}
NC3	5.04×10^7	59.0	5.01×10^{-3}
NC5	5.81×10^7	60.5	5.78×10^{-3}

of cross-linking increases by the reactions among the acrylate groups grafted to the clay layer and those of monomers and oligomers during the photopolymerization. Moreover, the incorporation of IH-MMT clays postponed the gelation time to facilitate the cross-linking reaction, where the modified IH-MMT clay acted as a crosslinker in the polymer chain networks.

The influence of modified clay component on the other physical properties of polymer/IH-MMT nanocomposites is listed in Table 4. The tensile strength of the nanocomposites increases with elevating the IH-MMT clay loading, which is in agreement with the results obtained by DMTA, where an increase in E' was observed in the presence of clay. However, the percent elongation decreases as the polymer chains in nanocomposites are restricted by the exfoliated clay layer, resulting in the decreased degree of freedom. It can be seen that, as the clay component increases, the enhancement of abrasion resistance is obtained for the good compatibility and interactions between the clay layer and the polymer matrix. The pendulum and pencil hardness were used to determine the hardness of the nanocomposite films; they correlated not only with the composition but also with the crosslink

Table 4
Properties of the pure polymer and polymer/IH-MMT nanocomposites

Sample	Tensile strength (MPa)	Elongation at break (%)	Abrasion resistance (mg)	Persoz hardness (s)	Pencil hardness
Pure polymer	8.2	30	12.3	85	2H
NC1	8.8	28	11.5	91	2H
NC3	9.3	25	9.6	99	3H
NC5	9.9	22	7.8	110	4H

network density of the nanocomposites. As listed in Table 4, the pendulum hardness and pencil hardness of the UV-cured pure polymer films are 85 s and 2H, respectively. With the addition of 1, 3, 5 wt% IH-MMT in the cured films, the values go up to 91, 99, 110 s and 2H, 3H, 4H, respectively. Compared with the pure polymer film, the pendulum and pencil hardness increase with increasing the IH-MMT clay loading in the nanocomposite film. It can be explained by the good compatibility of IH-MMT clay with the polymer matrix and the high effective crosslink density of the polymer/clay nanocomposites.

4. Conclusion

In conclusion, a novel method was developed to prepare exfoliated UV-curable polymer/clay nanocomposites. By the reaction between IPDI-HEA and hydroxyl groups of silicate layer, a high percentage of IPDI-HEA was grafted to the MMT layer which facilitated to exfoliate the clay layer during the photopolymerization. We anticipated that this new method can be applicable to a wide variety of clays and polymer systems for preparing polymer/clay nanocomposites.

Acknowledgment

The financial support of National Natural Science Foundation of China (No. 50633010) is gratefully acknowledged.

References

[1] Messersmith PB, Giannelis EP. Chem Mater 1994;6:1719.
[2] Lan T, Kaviratna PD, Pinnavaia TJ. Chem Mater 1995;7:2144.
[3] Wang Z, Pinnavaia TJ. Chem Mater 1998;10:1820.
[4] Yu YH, Lin CY, Yeh JM, Lin WH. Polymer 2003;12:3553.
[5] Yano K, Usuki A, Okada A, Kurauchi T, Kamigaito O. J Polym Sci: Polym Chem 1993;31:2493.
[6] Xie W, Gao ZM, Liu KL, Pan WP, Vaia R, Hunter D, et al. Polymer 2001;8:339.
[7] Aranda P, Hitzky ER. Chem Mater 1992;4:1395.
[8] Okada O, Kawasumi M, Usuki A, Kojima Y, Kurauchi T, Kamigaito O. Mater Res Soc Symp Proc 1990;171:45.
[9] Wang Z, Lan T, Pinnavaia TJ. Chem Mater 1996;8:2200.
[10] Kornmann X, Lindberg H, Berglund LA. Polymer 2001;42:1303.
[11] Wang K, Chen L, Wu JS, Tho ML, He CB, Yee AF. Macromolecules 2005;38:788.
[12] Kong D, Park CE. Chem Mater 2003;15:419.
[13] Chen B, Liu J, Chen HB, Wu JS. Chem Mater 2003;16:4864.
[14] Lu JK, Ke YC, Qi JN, Yi XS. J Polym Sci: Polym Phys 2001;39:115.
[15] Wang K, Wang L, Wu JS, Chen L, He CB. Langmuir 2005;21:3613.
[16] Messersmith PB, Giannelis EP. J Polym Sci: Polym Chem 1995;33:1047.
[17] Fu X, Qutubuddin S. Polymer 2001;42:807.
[18] Ghosh AK, Woo EM. Polymer 2004;45:4749.
[19] Vaia RA, Sauer BB, Tse OK, Giannelis EP. J Polym Sci: Polym Phys 1997;35:59.
[20] Tyan HL, Liu YC, Wei KH. Chem Mater 1999;11:1942.
[21] Lee DC, Jang LW. J Appl Polym Sci 1996;61:1117.
[22] Lin KF, Lin SC, Chien AT, Hsieh CC, Yen MH, Lee CH, Lin CS, et al. J Polym Sci: Polym Chem 2006;44:5572.
[23] Zahouily K, Benfarhi S, Bendaikha T, Baron J, Decker C. Proc Rad Tech Europe 2001:583.
[24] Zahouily K, Decker C, Benfarhi S, Baron J. Proc Rad Tech North Am 2002:309.
[25] Uhl FM, Davuluri SP, Wong SC, Webster DC. Chem Mater 2004;16:1135.
[26] Uhl FM, Davuluri SP, Wong SC, Webster DC. Polymer 2004;45:6175.
[27] Uhl FM, Webster DC, Davuluri SP, Wong SC. Eur Polym J 2006;42:2596.
[28] Dean KM, Bateman SA, Simons R. Polymer 2007;48:2231.
[29] Asif A, Huang CY, Shi WF. Colloid Polym Sci 2004;12:200.